Photophysical Processes in 'Supramolecular Balls' Formed by Lanthanide Chloride with 2,2′-Bipyridine

by **Lada N. Puntus***

Laboratory of Molecular Nanoelectronics, Institute of Radio Engineering & Electronics, Russian Academy of Sciences, 11-7 Mokhovaya, RU-125009 Moscow (e-mail: lada_puntus@mail.ru)

With gratitude to Prof. *Jean-Claude G. Bünzli* for induced interest to supramolecular lanthanide chemistry

The europium complex $[EuCl_2(bpy)_2(H_2O)_2]Cl \cdot 1.25\ C_2H_6O \cdot 0.37\ H_2O$, where bpy is 2,2′-bipyridine, was synthesized and investigated with the aim to relate its molecular geometry and crystal packing to the efficiency of energy-transfer processes. The presence of H-bonds between noncoordinated Cl^- ions and coordinated H_2O molecules leads to the formation of discrete trimers assembled by a number of $C-H\cdots Cl$ and stacking interactions into 'supramolecular balls' which contain Cl^- ions and solvate molecules (H_2O and EtOH). The additional stabilization of the complex is due to intramolecular $N\cdots C$ interactions between two bpy ligands that causes some shortening of the Eu–N bonds. Deciphering the luminescence properties of the Eu complex was performed under consideration of both the composition of the inner coordination sphere and the peculiarities of the crystal packing. The influence of the latter and the bpy orientation on the energy of the ligand → Eu charge-transfer state (LMCT) was established, and an additional excited state induced by the π-stacking interaction (SICT) was identified.

Introduction. – Weak noncovalent forces (H-bonding, coordination bonds, electrostatic and charge-transfer attractions, aromatic π-stacking interaction, *etc.*) are the subject of intensive study as a new approach of developing materials science [1]. In coordination chemistry, these weak interactions are important in determining the conformations, the selectivities of the reactions, and the crystal structures of metal complexes [2]. The $\pi-\pi$ and $CH-\pi$ interactions are noncovalent forces which contribute to self-assembly and/or recognition processes when extended structures are formed from building blocks with aromatic moieties [3]. Recently it has been reported that the photophysical properties of transition-metal complexes are affected by intermolecular $\pi-\pi$ and $CH-\pi$ interactions [4]. The introduction of rare-earth metals into self-assembling molecular architectures can lead to the design of advanced luminescent materials. The unique ability of the rare-earth metals to emit well-defined narrow bands in different spectral ranges from VIS to near-IR with relatively long lifetimes and high quantum yields [5] makes them perfect candidates for many fields of materials science. In spite of the fact that numerous lanthanide complexes have been intensively studied to find a method to manage the efficiency of photophysical processes, many questions of the influence of the supramolecular structure on the properties of the lanthanide systems are still open, and no systematic studies of the effect of noncovalent interactions on photophysical properties have been performed.

The 2,2′-bipyridine (bpy) is a well known ligand of highly luminescent complexes with transition and rare-earth metals. In the former case, diimine complexes of

transition metals serve as effective sensitizers for photochemical reactions involving a net electron transfer [6]. In the latter case, the intense absorption band of bpy in the near-UV region and the ability to efficiently transfer energy onto the Ln excited states (antenna effect [7]) lead to an effective intramolecular energy-transfer process [5][8]. Moreover, there is a great interest in heterometallic d-f complexes containing bpy in which the strong absorption of light by metal-to-ligand charge-transfer (MLCT) transitions associated with d-block fragments (typically of Ru^{II}, Os^{II}, Re^{I}, or Pt^{II}) is used to sensitize luminescence from rare-earth ions with low-energy f-f excited states [9]. Another interest of 2,2′-bipyridine is due to its ability to form $\pi-\pi$ stacking dimers or oligomers, as well as other supramolecular architectures, by weak ligand–ligand, cation–anion, and anion–anion interactions [3]. It was found that these interactions can noticeably influence both the photophysical properties of the resulting edifices by creating additional excited states and the formation of nanoparticles, even [2][10][11].

Thus, the purpose of the current research was to elucidate some correlations between the photophysical properties of the europium system and the supramolecular architecture which is formed by noncovalent interactions by means of the example of europium chloride with 2,2′-bipyridine. Recently an isomer series of lanthanide chlorides with bpy was investigated [12], but the presented complex $[EuCl_2(bpy)_2(H_2O)_2]Cl \cdot 1.25\ C_2H_6O \cdot 0.37\ H_2O$ (**1**) was characterized only by X-ray crystal-diffraction since the obtained quantity of complex was unsufficient. The further developing of both the method and the conditions of crystallization now allowed to overcome this. The published isomers are highly luminescent and exhibit a row of peculiarities of the energy-transfer process, including the participation of a ligand-to-metal charge-transfer (LMCT) state and a stacking-induced charge-transfer (SICT) state in the sensitization of Ln^{III} luminescence. Therefore, the in-depth investigation of one example of this series is practically important for a thorough understanding of the energy-transfer processes in Ln systems which are self-assembled by noncovalent interactions. Since bpy is a part of numerous luminescent systems, the photophysical properties of its crystals were studied as well.

Results and Discussion. – In view of the below consideration of the influence of the molecular geometry and crystal packing on peculiarities of the luminescence spectra and energy-transfer processes, some distinct structural differences between the complexes $[EuCl_2(bpy)_2(H_2O)_2]Cl \cdot 1.25\ C_2H_6O \cdot 0.37\ H_2O$ (**1**) and $[EuCl_2(bpy)_2(H_2O)_2]Cl$ (**2**) are presented first.

Molecular Structure and Crystal Packing. According to X-ray diffraction data [12], the complex **1** crystallizes with solvate molecules of H_2O and EtOH (*Fig. 1*, *Table 1*). The Eu^{III} is coordinated by four N-atoms of two bpy ligands, two Cl-atoms, and two O-atoms of coordinated H_2O. The europium coordination number is 8. The coordination geometry can be described as a distorted square antiprism both bases of which are composed of one Cl^- ion, one H_2O molecule, and one bpy ligand. Although the complex is formally characterized by C_2 symmetry, the Eu-ion in the crystal occupies the general position, and its symmetry is C_1. The distortions of the coordination polyhedron are almost negligible in complex **1**. Indeed, the mean displacement of atoms from the antiprism bases and dihedral angle between the bases are 0.01–0.06 Å and 0.3°, respectively. These distortions are more pronounced in **2**, where the mean

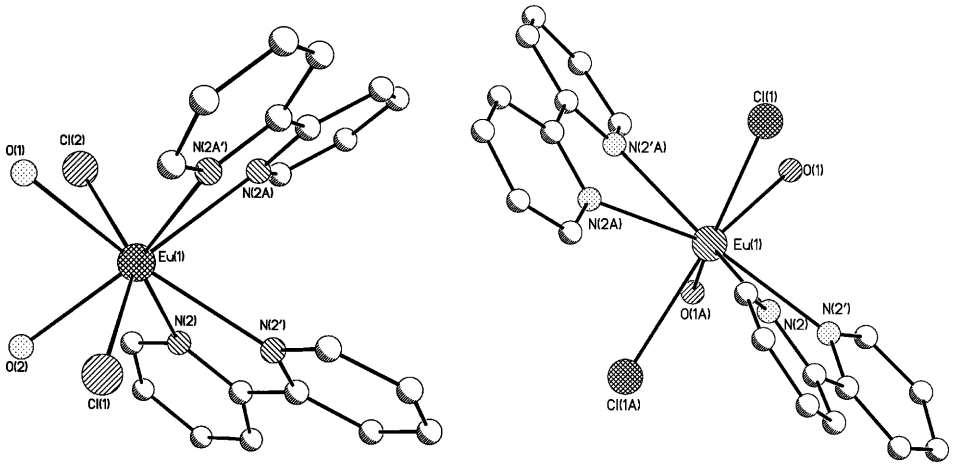

Fig. 1. *General view of the cations of* **1** (left) *and* **2** (right) *according to* [12]. Arbitrary atom numbering.

Table 1. *Selected Bond Lengths in the Europium Complexes* **1** *and* **2** [12]

1		**2**		Average bond lengths [Å]		
Eu(1)–O(2)	2.405(3)	Eu(1)–O(1)	2.398(2)	Eu–Cl	2.714	2.710
Eu(1)–O(1)	2.417(3)			Eu–O	2.411	2.398
Eu(1)–N(2A)	2.551(3)			Eu–N	2.587	2.599
Eu(1)–N(2′)	2.586(3)	Eu(1)–N(2)	2.613(3)			
Eu(1)–N(2A′)	2.602(3)	Eu(1)–N(2′)	2.586(2)			
Eu(1)–N(2)	2.608(3)					
Eu(1)–Cl(2)	2.7074(9)	Eu(1)–Cl(1)	2.7097(8)			
Eu(1)–Cl(1)	2.7208(9)					

displacement of atoms from the antiprism base and dihedral angle between the bases are 0.18 Å and 9.8°, respectively.

The main peculiarity of complex **1** is that the bpy ligands are located directly under each other with the shortened intramolecular N(2A)···C(1′) contact equalling 3.572(2) Å, while in other chloro complexes, the bpy are positioned in opposite directions [12]. The intramolecular N···C interactions between the two bpy ligands cause some shortening of the Eu(1)–N(2A) and Eu(1)–N(2′) distances with respect to the Eu(1)–N(2) and Eu(1)–N(2A′) ones. It should be noted that the same intramolecular contacts in bpy complexes was observed only for lanthanide nitrates according to the database of the *Cambridge Crystallographic Data Center*.

In complex **1**, H-bonds lead to the formation of discrete trimers (*Fig. 2*) assembled by a number of C–H···Cl contacts and stacking interactions into 'supramolecular balls' which domain Cl^- ions and solvate molecules (H_2O and EtOH). The 3D-framework formed by the O–H···Cl and stacking interactions in the crystal of **1** is presented in *Fig. 2* (right). The possible reason of such an unusual 'zeolite-type' packing in **1** is the presence of EtOH solvate molecules or more precisely, aggregates of EtOH with noncoordinated Cl^- ions $[Cl(EtOH)_4]^-$, that are situated with in the

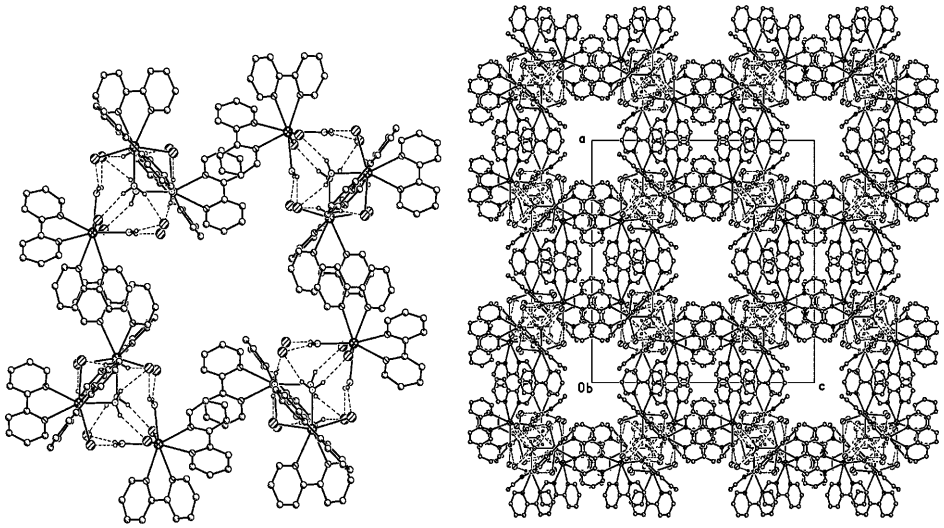

Fig. 2. *Fragments of H-bonded trimers in* **1** (left) *and 3D-framework of* **1** (right). In both views, disordered solvate molecules as well as $[Cl(EtOH)_4]^-$ aggregates that serve as the filling of the cavities are omitted for clarity.

relatively big channels (*ca.* 6×15 Å). Thus, we may propose that addition of other alcohols with longer alkane chains can be a way to vary the supramolecular organization of europium-containing cations.

Some differences between complexes **1** and **2** concerning the features of net charge distribution should be noted. In **2** coordinated Cl^- ions participate in H-bonds only with coordinated H_2O molecules. Taking into account that coordinated H_2O molecules are characterized by a negative total charge [11], we may expect that such a type of H-bonds, *i.e.*, $O-H\cdots Cl$, will reduce the charge transfer from the Cl^- ion to H_2O. This assumption coincides well with the decrease of the $Eu-Cl$ bond lengths in **1** and **2** (*Table 1*). At the same time, we cannot exclude the possible role of a noncoordinated Cl^- ion, which in the case of **1** participates in H-bonds only with coordinated H_2O molecules and thus can decrease the positive charge of the cationic species.

Metal-Centered Luminescence. Upon excitation at 330 nm, the emission spectra of complex **1** (77 and 300 K) show the typical narrow bands corresponding to the Eu^{III} $^5D_0 \rightarrow {}^7F_J$ ($J = 0-4$) transitions (*Fig. 3*). Both spectra are quite similar, and the slightly worse spectrum resolution at 300 K is caused by temperature-dependent line broadening. The luminescence spectrum formed by the transitions from the $^5D_1$ level of Eu^{III} was also detected (*Fig. 4*).

The intensities and *Stark* splittings of the $^5D_0 \rightarrow {}^7F_J$ transitions are influenced by the strength and symmetry of the ligand field. Although the symmetry of the first coordination sphere gives the main contribution to this field, also outer-sphere interactions have to be taken into account [13]. The role of the latter interactions and net charge distribution increases in complexes which are similar to **1**, due to the presence of the H-bond system between noncoordinated and coordinated Cl^- ions and H_2O molecules.

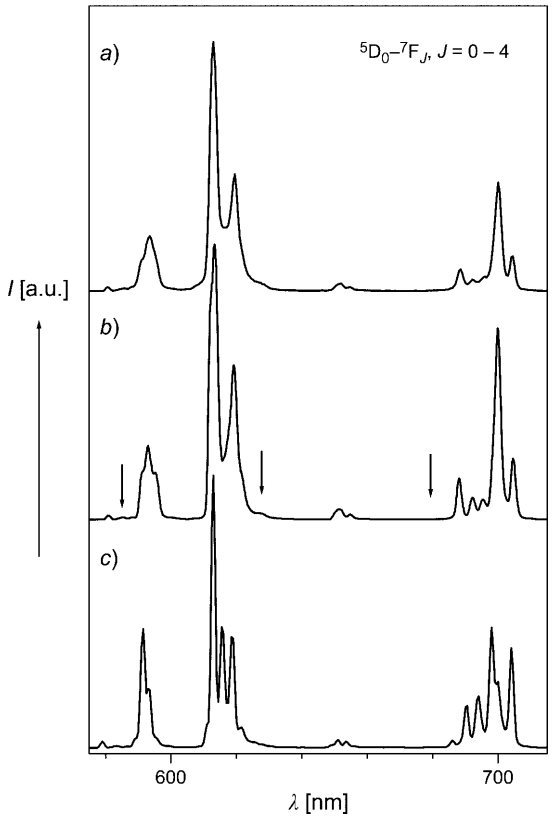

Fig. 3. *Luminescence spectra of* a) **1** *at 300 K,* b) **1** *at 77 K, and* c) **2** *at 77 K*. The arrows denote the regions of vibronic sidebands.

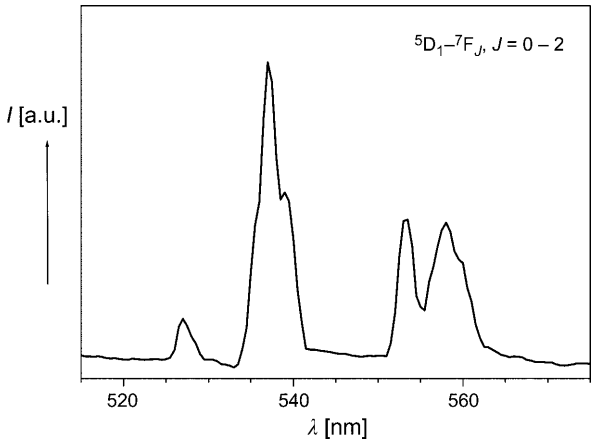

Fig. 4. *Luminescence spectrum of* **1** *in the region of the* $^5D_1 \rightarrow {}^7F_J$ *transitions at 77 K*

A forbidden $^5D_0 \rightarrow {}^7F_0$ transition of Eu^{III} situated at 581 nm (*Fig. 3*) cannot be split by the ligand field and, therefore, serves as a probe of the number of nonequivalent luminescence centers. This transition is nondegenerated in complex **1** that indicates the presence of only one type of Eu environments in the crystal. A magnetic-dipole $^5D_0 \rightarrow {}^7F_1$ transition of **1** centered at 593 nm is largely independent of the Eu^{III} chemical environment. An electric-dipole $^5D_0 \rightarrow {}^7F_2$ transition with the most intense *Stark* component at 613 nm is extremely sensitive to the symmetry of the coordination sphere and called 'hypersensitive'. The ratio of the integrated intensity of the $^5D_0 \rightarrow {}^7F_2$ transition to the one of the $^5D_0 \rightarrow {}^7F_1$ transition is a measure for the symmetry of the coordination sphere [14]. In a centrosymmetric environment, the magnetic-dipole $^5D_0 \rightarrow {}^7F_1$ transition is dominating and the above-mentioned ratio < 1, while the distortion of the symmetry around the metal center causes an intensity enhancement of the $^5D_0 \rightarrow {}^7F_2$ transition. In complex **1**, this ratio is 3.6 indicating a significant deviation from an inversion center. Interestingly, the luminescence spectrum of **2** which is an isomer of **1** (*Fig. 3*) has a remarkably higher ratio of the integrated intensities of the $^5D_0 \rightarrow {}^7F_J$ transitions ($J = 2, 4$) to one of the $^5D_0 \rightarrow {}^7F_1$ transition and three *Stark* components in the $^5D_0 \rightarrow {}^7F_2$ transition instead of two ones observed in this transition for complex **1**. These facts reveal that the deviation from an inversion center in **2** is more pronounced than in **1**.

Due to the shielding of the 4f orbitals from the environment by an outer shell of 5s and 5p electrons, the values of the crystal-field splittings are as small as 120, 260, and 340 cm^{-1} for the ^7F_J states where $J = 1$, 2, and 4, respectively. Interestingly, the general splitting of the $^7F_4$ manifold is remarkably larger in **2** (360 cm^{-1}) than in **1**, which can be produced by a different charge distribution around Eu^{III}. In complex **2**, there is a noncoordinated Cl^- ion with the Eu–Cl^- distance of 4.26 Å, which is absent in **1** where all noncoordinated Cl^- ions are situated further away from Eu^{III} than 5 Å [13]. The number of *Stark* components is 1, 3, 2, 2, and 5 *vs.* the maximum possible ones of 1, 3, 5, 7, and 9 for the ^7F_J levels ($J = 0–4$), respectively. Therefore, the site symmetry of the Eu^{III} in **1** could be considered as a low point group not higher than C_{2v}. Potentially, the high intensity of the first *Stark* component of the $^5D_0 \rightarrow {}^7F_2$ transition (613 nm, *ca.* 30% of the total integrated intensity, hwfw (full width-at-half-height) = 80 cm^{-1}) can successfully be used for obtaining a relatively high color purity. The luminescence-decay curves obtained from time-resolved luminescence experiments could be fitted monoexponentially with time constants in the range of microseconds. The luminescence lifetime of the $^5D_0$ level of **1** at 77 K and 300 K is 0.37 ± 0.02 and 0.35 ± 0.02 ms, respectively. These values are in line with the presence of four O–H oscillators (two H_2O molecules) in the Eu^{III} coordination sphere, in accordance with the X-ray diffraction data.

To perform a complete assignment of the *Stark* components and to exclude the possible mixture of them with vibronic satellites, the latter ones were analyzed as well. Vibronic sidebands are associated with electronic transitions, which could be analyzed in terms of metal-to-ligand bond strength. The vibronic sideband of the $^5D_0 \rightarrow {}^7F_0$ transition (region 580–590 nm (17240–16950 cm^{-1})) is formed mostly by the intense bands assigned to $\nu(Eu^{3+}–Cl^-)$ vibrations but the contribution of $\nu(Eu^{3+}–O)$ is also possible. These vibrations have the same frequencies as those observed for **2** (130, 215 cm^{-1}) [12], which is in line with the similar Eu–Cl and Eu–O bond lengths in both

complexes (*Table 1*). Other intense vibronic sidebands are observed in the low-frequency region of the $^5D_0 \rightarrow {}^7F_2$ and $^5D_0 \rightarrow {}^7F_3$ transitions (630–650 nm (15900–15400 cm^{-1}) and 660–690 nm (15150–14550 cm^{-1}), respectively). The frequencies of 560 (δ (CH) out-of-plane), 795 (δ (ring) in-plane), and 1440 and 1495 cm^{-1} (ν (C=C), (C=N), δ (CH)) [15] are presented in these sidebands. The final list of electronic sublevels of the ^7F_J ($J = 0-4$) manifold based on the analysis performed is presented in *Table 2*.

Table 2. *Crystal-Field Splitting of the ^7F_J Levels and Their Barycenters* (bc)

$^{2S+1}L_J$	E^a) [cm^{-1}]	B [cm^{-1}]	$^{2S+1}L_J$	E^a) [cm^{-1}]	B [cm^{-1}]
$^7F_1$	296	354	$^7F_3$	1863	1898
	349			1945	
	416		$^7F_4$	2677	2843
$^7F_2$	879	995		2761	
	906			2834	
	1063			2926	
	1132			3018	

a) Energy calculated from the $^5D_0$ level.

Energy-Transfer Process. As the first step, the photophysical properties of bpy crystals were considered. The fluorescence and phosphorescence spectra of bpy crystals are given in *Fig. 5*. The energy of the singlet excited state (S_1) and the triplet state (T) of bpy determined from the 0–0 transition amounts to 330 nm (30300 cm^{-1}) and 470 nm (21200 cm^{-1}), respectively. The band assigned to the excited singlet state has a fine structure with vibronic progression of *ca.* 1300 cm^{-1}, probably attributable to an in-plane deformation vibration of the bpy rings (δ (ring) in-plane) [15]. Although bpy is a well known molecule, the direct measurement of the excited-state lifetimes (τ_S, τ_T) by time-correlated single-photon counting (TCSPC) is lacking. The lifetimes of the fluorescence and phosphorescence measured with TCSPC are 3.4 ± 0.2 ns and 300 ± 5 ms, respectively, for bpy crystals.

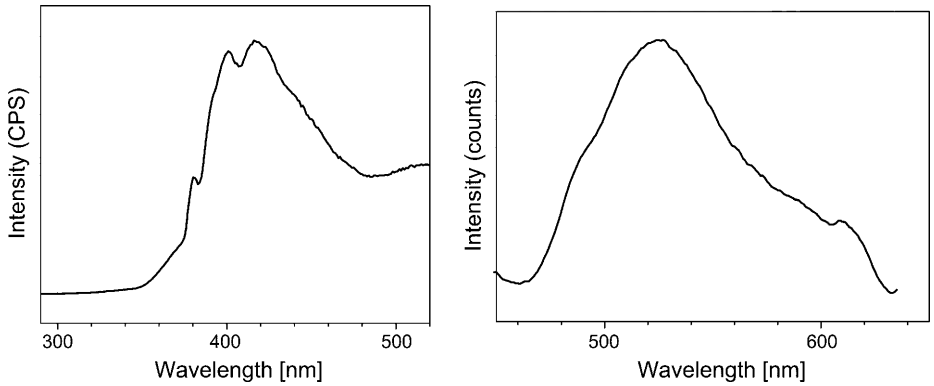

Fig. 5. *Fluorescence* (left) *and phosphorescence* (right) *spectra of bpy crystals*

The luminescence sensitization in lanthanide-containing systems by the energy transfer from ligand excited states to the resonance states of Ln^{III} can occur in different ways. The favorite mechanism, simplified, involves ligand excitation by the absorption of UV energy to an excited singlet state, followed by energy migration *via* nonradiactive intersystem crossing to a ligand triplet state ($\Delta E_1 = E(S_1) - E(T)$) and energy transfer from the triplet state to a resonance state of the Ln^{3+} ion, from which the emission occurs ($\Delta E_2 = E(T) - E(^5D_J)$, where $J = 0$ for the Eu^{3+}) [16]. In principal, direct transfer from the singlet S_1 state is also possible but seems to be less important for Eu^{III} than for Tb^{III} [17]. Moreover, in the case of Eu^{III} complexes, a photon-induced electron transfer (LMCT) may also play a role in the deactivation of the singlet excited state. Indeed, instead of radiative decay to the ground state, or intersystem crossing to the triplet state, an electron is transferred to the Eu^{III} center upon excitation of the antenna into its singlet excited state, resulting in the transient formation of an antenna radical cation and Eu^{II} [18]. One of the reasons for the possible occurrence of this competing process is the low reduction potential of Eu^{III} in comparison with other trivalent lanthanide ions [19]. Therefore, there is no doubt that the singlet and triplet states of the ligand as well as the LMCT state play an important role for an effective energy transfer in europium systems.

Since the Gd^{3+} ion has no energy levels below 310 nm (32000 cm^{-1}), it can be used for the energy estimation of the excited states of coordinated ligands. The energy of the singlet excited state (S_1) of 330 nm (30300 cm^{-1}) of bpy was determined from the 0–0 transition which is clearly observed in the luminescence spectrum of the Gd complex with bpy at 300 K (*Fig. 6*). The luminescence spectrum of this Gd complex at 77 K shows a strong phosphorescence band near to weak fluorescence band. The energy of the lowest triplet state (T) of 455 nm (21980 cm^{-1}) was determined from the 0–0 transition in the phosphorescence spectrum (*Fig. 6*). The excited triplet state displays a fine structure with vibronic progression of *ca.* 1150 cm^{-1} probably attributable to the deformation vibrations of CH groups (δ(C–H)) [15]. Interestingly, the phosphorescence band of **1** has slightly shifted to the blue (*ca.* 700 cm^{-1}) in comparison with the

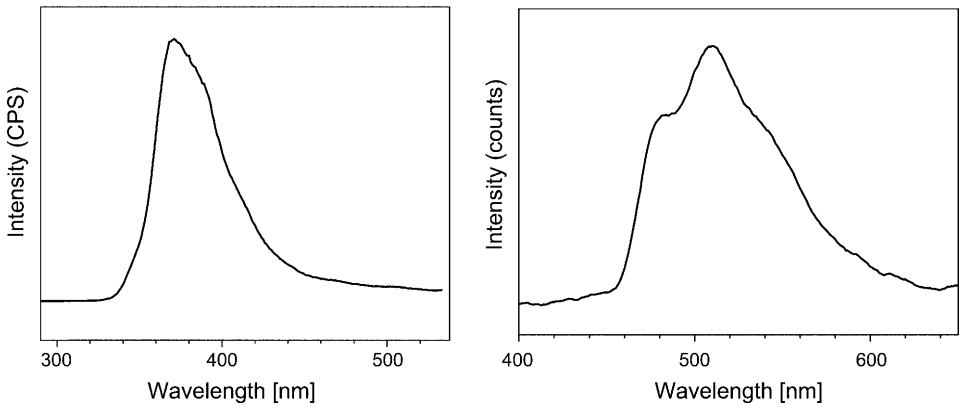

Fig. 6. *Fluorescence* (left) *and phosphorescence* (right) *spectra of the Gd complex with bpy*

phosphorescence band of the free bpy. It can be caused by the exchange of the s-*trans*- to the s-*cis*-bpy isomer upon coordination by Eu^{3+} along with a deviation of bpy from planarity and an overlap of the π-systems of the pyridine rings due to an intramolecular interaction between the two coordinated bpy ligands. Additionally, the presence of emission from the $^5D_1$ state which converts nonradiatively into the $^5D_0$ state and radiatively to the ^7F_J manifold (*Fig. 4*) is logical for the sensitized Eu^{III} emission when the donating triplet level of bpy is above the $^5D_1$ level of Eu^{III}. The latter is in line with the value measured for the triplet state energy. The lifetimes of the fluorescence and phosphorescence measured with TCSPC for the Gd complex with bpy are 3.2 ± 0.1 ns and 25 ± 2 ms, respectively.

Scanning the excitation wavelength while monitoring the intensity of the Eu^{III} emission at 613 nm (the strongest component of the $^5D_0 \rightarrow {}^7F_2$ transition) shows which transitions from the ground-state directly or indirectly lead to population of the $^5D_0$ state of Eu^{III}. The excitation spectra of the Eu^{III} complex display, in addition to the narrow f-f transitions ($^5L_6 \leftarrow {}^7F_0$, $^5D_{2,1,0} \leftarrow {}^7F_0$, *Fig. 7*), a broad band extending from 265 to 450 nm with an intense component at 335 nm (29850 cm^{-1}), two smaller ones at *ca.* 360 (27780 cm^{-1}) and 375 nm (26740 cm^{-1}), and a weak shoulder with long-wavelength edge at *ca.* 450 nm (22200 cm^{-1}). To distinguish these bands, the multi-peaks fit procedure was performed, and three states were found (*Fig. 8*). The first 335 nm-band is attributed to the first excited S_1 state [12]. Clarification of the origin of the two other bands comes from the analysis of the excitation spectrum of complex **2** according to which they correspond to the LMCT state (375 nm) with broadened vibronic structure (a case of medium electron–phonon interaction). The observed frequency of *ca.* 1010 cm^{-1} is attributed to the 'breathing' symmetric vibrational mode of the bpy rings. The last band with long-wavelength edge at *ca.* 450 nm can be tentatively assigned to an intraligand charge-transfer state induced by a stacking interaction (SICT) state. Owing to the superposition of several excited states, the maximum of the band corresponding to the SICT state in **1** is covered. However, a similar state with a maximum at *ca.* 370 nm (27030 cm^{-1}) has been previously identified in the analogous series of complexes, with bpy and phen [11][12]. In these complexes strong π-stacking interaction between heterocyclic diimine ligands causes a charge redistribution in these ligands, and as a result, an intraligand charge-transfer state was observed in the excitation spectra. It is noteworthy that the presence of the SICT state was established by both the analysis of the experimental charge-density distribution [11] and time-dependent density-functional-theory (TD-DFT) calculations [12]. By the latter it was demonstrated that *i*) the C···C separation affects the SICT-state energy to a greater degree than the overlap area of the aromatic rings, and *ii*) the stronger stacking interaction leads to a lower energy of the SICT. In complex **1**, the C···C separation is even shorter than in **2** (3.325 *vs.* 3.373 Å), this correlates well with the long-wavelength edge of the proposed SICT state.

Surprisingly, in spite of the quite similar bond-length distribution in complexes **1** and **2** including the Eu–Cl ones, the energy of their LMCT states is remarkable different ($\Delta =$ *ca.* 35 nm (2670 cm^{-1})). Taking into account the electronegativity of Eu^{III}, uncorrected for spin correlation, $\chi_{uncorr}(Eu) = 1.99$ [20] and $E_{CTS} \approx 30000 \cdot [\chi_{opt}(X) - \chi_{uncorr}(Eu)]$ cm^{-1} [21], the optical electronegativity of the ligand χ_{opt} in **1** amounts to 2.88. The same parameter equals 2.97 in **2**. The last value is quite similar to

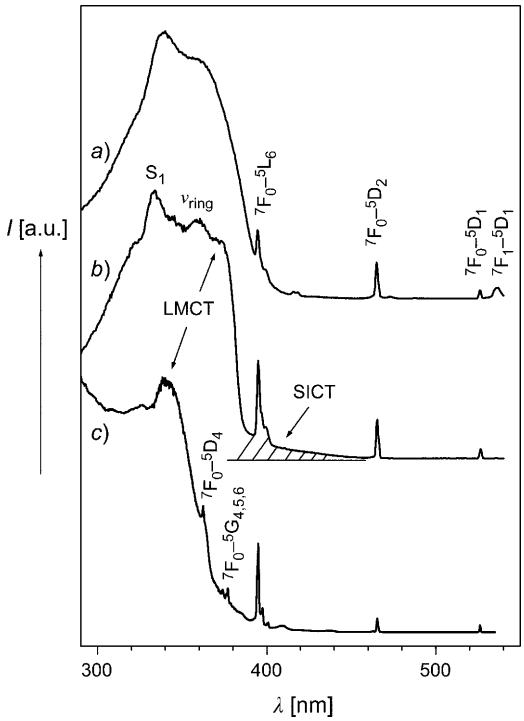

Fig. 7. *Excitation spectra of* a) **1** *at 300 K,* b) **1** *at 77 K, and* c) **2** *at 77 K*

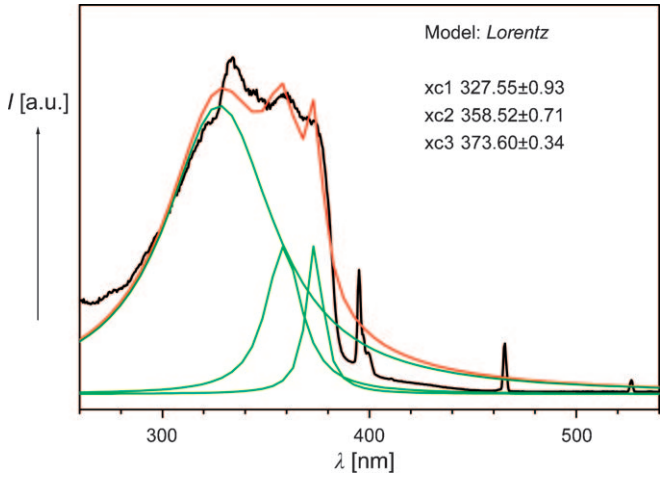

Fig. 8. *The multi-peaks fit procedure for the excitation spectrum of* **1** *at 77 K*

Pauling's electronegativity for chlorine (3.0), and charge transfer from Cl^- to Eu^{III} causes mainly the LMCT state. This assignment is also confirmed by structural data of **2**. Firstly, the presence of the H-bonds between the coordinated Cl^- ions and

coordinated H_2O molecules in **2** leads to short the Eu–Cl bonds (*ca.* 2.71 Å). Secondly, the noncoordinated Cl^- ions participate in H-bonds only with coordinated H_2O molecules, which results in a decrease in the positive charge of the metal ion. Therefore, it is reasonable that the LMCT state is formed mostly by the $Cl^- \rightarrow Eu^{3+}$ charge transfer. Taking into account that the H-bonding pattern in the 'supramoleculer balls' is almost the same (*Fig. 2*) as in **2** as well as the Eu–Cl bond lengths, the decreasing χ_{opt} in complex **1** seems to be caused by the charge redistribution originating from the special position of the bpy ligands (the short contact between the bpy can lead to intramolecular interaction). Additional confirmation of the participation of the bpy ligands in the charge transfer producing the LMCT state at 375 nm is the appearance of the 'breathing' vibration of the bpy rings in the vibronic sideband of this state. It is worth stressing that the χ_{opt} found is the electronegativity of the whole Eu^{III} environment in complex **1**. Hence the unique properties of the Eu^{III} system presented provide an unusual opportunity to detect experimentally the LMCT state with the vibronic wing and shed more light on the influence of the whole chemical environment of the Eu^{III} on the energy of this state.

Normalizing the excitation spectra with respect to the integrated intensity of the magnetic dipole $^5D_1 \leftarrow {}^7F_0$ transition allows one to estimate the relative efficiency of excitation through absorption bands of ligands *vs.* direct f-f excitation and indicates the remarkably reduced efficiency in **1** *vs.* **2** at 77 K. This fact is in line with the excitation deactivation *via* the lower-lying LMCT state in **1**. The intrinsic quantum yield of the Eu^{III}-centered emission $Q_{EU}^{EU} = 15\%$ calculated by means of *Werts*' formula [22][1]) has the same trend and is lower in **1** in comparison with **2** ($Q_{EU}^{EU} = 22\%$ [12]).

The information gained from the above analysis of the energy-transfer processes may be summarized as follows. The energy differences between the S_1 and LMCT, and S_1 and T states of **1** amount to 3100 and 7850 cm^{-1}, respectively. The latter difference (ΔE_1) remarkably exceeds the optimum value which should be *ca.* 5000 cm^{-1} for effective intersystem conversion [23]. The former difference also cannot be considered as intermediate 'stair' promoting effective intersystem conversion as in the case of complex **2** [12]. The LMCT state probably competes with the intersystem conversion to the triplet state in complex **1**. In general, the deactivation of the LMCT state does not result in the population of the Eu^{III} $^5D_1$ excited state, and a photon-induced electron-transfer process reduces the overall luminescence quantum yield [24]. However, the presence of the SICT state with a long-wavelength wing until 450 nm can promote the preservation of efficient intersystem conversion to the triplet state ($E(T) = 455$ nm). The energy difference between the T and $^5D_0$ levels ($\Delta E_2 = 4760$ cm^{-1}) is also out of the optimum range, but taking into account the presence of emission from the $^5D_1$ level, the energy gap became much more near to optimum ($\Delta E_2 = 2980$ cm^{-1}). In such a way, the data presented clearly demonstrate that crystal packing as well as molecular geometry influence the energy of the LMCT and SICT states and, as a consequence, the efficiency of energy-transfer processes in Eu-containing system.

---

[1]) $Q_{Eu}^{Eu} = \tau_{obs}/\tau_R = \tau_{obs} \cdot A_{MD,0} \cdot n^3 \cdot (I_{tot}/I_{MD,0})$, where $A_{MD,0}$ is a constant spontaneous emission probability (14.65 s^{-1} for Eu^{III}), n the refractive index, I_{tot} the total area of the emission spectrum ($^5D_0 \rightarrow {}^7F_J$, $J = 0-6$), and $I_{MD,0}$ the $^5D_0 \rightarrow {}^7F_1$ band area. The refractive index was taken as 1.5 for all cases.

Conclusions. – The detailed analysis of the photophysical properties of the Eu^{III} complex **1** with Cl^- and two 2,2′-dipyridine ligands in the inner coordination sphere assembled into 'supramolecular balls' containing uncoordinated Cl^- and solvate molecules allowed us to decipher the influence of structural peculiarities and crystal-packing effects on these properties. The strength and symmetry of the crystal field in complex **1** is significantly different from the ones in the isomeric complex **2** having a completely similar coordination sphere with only one exception, namely a different orientation of the bpy ligands relative to each other in **1** promoting the interaction between them.

The photophysical processes leading to the sensitized luminescence of Eu^{III} in complex **1** correlate well with the structure and the peculiarities of the chemical-bonding pattern both in the inner and outer coordination spheres. As a consequence, two additional excited charge-transfer states were found, namely a ligand-to-metal and a stacking-induced charge-transfer state (LMCT and SICT, resp.). The pronounced π-stacking interaction observed in **1** causes a redistribution of the charges on the bpy ligands and leads to the appearance of the SICT, the energy of which correlates with the strength of the π-stacking interactions. The energy determined for the LMCT state witnesses that not only Cl^- ions contribute to this charge transfer but also the bpy ligands owing to their specific orientation.

The now established influence of the Eu^{III} chemical environment and supramolecular organization in Eu-containing systems on efficiency of energy transfer processes resulting in appearance of the additional excited states (LMCT and SICT) opens up a new approach for the tuning of the energy of the quenched states which can be used upon the molecular design of new luminescence systems.

This study was financially supported by the *Russian Foundation for Basic Research* (grants no. 09-03-00603, 09-03-12065, 10-03-00898), and the *Foundation of the President of the Russian Federation* (*Federal Program for the Support of Young Doctors*, Grant MD-172.2008.3 and MK-6026.2008.9). The author thanks Prof. *K. A. Lyssenko* for X-ray crystallography research.

Experimental Part

Materials and Methods. All reagents were purchased from *Aldrich* and used as received. All solvents were reagent grade and purified by standard techniques whenever required. Steady-state luminescence measurements in the VIS region were performed with a *Fluorolog-FL-3-22* spectrometer from *Horiba-Jobin-Yvon-Spex* which has a 475 W Xe lamp as the excitation source. The singlet- and triplet-excited-state lifetimes were measured by a standard experimental setup for time-correlated single-photon counting (TCSPC) [25] with laser excitation by the 282 and 340 nm *NanoLeds* from *Horiba Jobin Yvon IBH*. Luminescence lanthanide lifetimes (τ) were measured on samples put into quartz capillaries; they are averages of at least three independent measurements, which were achieved by monitoring the decay at the maxima of the emission spectra. The mono- or biexponential decays were analyzed with Origin® vs. 7.0. Attenuated total reflectance IR spectra: powdered samples; *Perkin-Elmer-Spectrum-One* FT-IR spectrometer.

Complexes. Lanthanide chlorides were treated with 2,2′-bipyridine in Ln/bpy 1:2 stoichiometric ratios (Ln = Eu and Gd) to give the following complexes, according to a procedure similar to the one used for the complexes with phen: $[EuCl_2(bpy)_2(H_2O)_2]Cl$ (**2**), $[EuCl_2(bpy)_2(H_2O)_2]Cl \cdot 1.25\ C_2H_6O \cdot 0.37\ H_2O$ (**1**), and $[GdCl_3(bpy)_2(H_2O)_3]$. Compound **1** was obtained during the preparation of single crystals and was not subjected to elemental analysis, but all spectroscopic measurements were performed on the crystals used for X-ray analysis. The Gd complex was doped by 2 mol-% of Eu^{III} for the spectral control of the content obtained.

Data of **2**: Yield 97%. Anal. calc. for $C_{20}H_{22}Cl_3EuN_4O_3$ (624.74): C 38.45, H 3.55, N 8.97; found: C 38.57, H 3.67, N 8.91.

Data of the Gd Complex. Yield 70%. Anal. calc. for $C_{20}H_{22}Cl_3GdN_4O_3$ (630.03): C 38.13, H 3.52, N 8.89; found: C 38.25, H 3.96, N 8.86.

REFERENCES

[1] C. Janiak, *Angew. Chem., Int. Ed.* **1997**, *36*, 1431; W. J. Hunks, M. C. Jennings, R. J. Puddephatt, *Inorg. Chem.* **2002**, *41*, 4590; M. Kondo, T. Yoshihitomi, H. Matsuzaka, S. Kitagawa, K. Seki, *Angew. Chem., Int. Ed.* **1997**, *36*, 1725; J. L. Manson, A. M. Arif, C. D. Incarvito, L. M. Liable-Sands, A. L. Rheingold, J. S. Miller, *J. Solid State Chem.* **1999**, *145*, 369.

[2] H. Tsubaki, S. Tohyama, K. Koike, H. Saitoh, O. Ishitani, *Dalton Trans.* **2005**, 385.

[3] C. Janiak, *J. Chem. Soc., Dalton Trans.* **2000**, 3885.

[4] F. Barigelletti, B. Ventura, J.-P. Collin, R. Kayhanian, P. Gaviña, J.-P. Sauvage, *Eur. J. Inorg. Chem.* **2000**, 113; J.-P. Collin, R. Kayhanian, J.-P. Sauvage, G. Calogero, F. Barigelletti, A. De Cian, J. Fisher, *Chem Commun.* **1997**, 775; L. B. Picraux, B. T. Weldon, J. K. McCusker, *Inorg. Chem.* **2003**, *42*, 273.

[5] J.-C. G. Bünzli, C. Piguet, *Chem. Soc. Rev.* **2005**, *34*, 1048.

[6] A. Guerzo, S. Leroy, F. Fages, R. Schmehl, *Inorg. Chem.* **2002**, *41*, 359; V. Balzani, F. Bolletta, M. Ciano, M. Maestri, *J. Chem. Educ.* **1983**, *60*, 447; T. J. Meyer, *Acc. Chem. Res.* **1989**, *22*, 163; M. Grätzel, *Coord. Chem. Rev.* **1991**, *111*, 167.

[7] S. I.Weissman, *J. Chem. Phys.* **1942**, *10*, 214.

[8] J.-C. G. Bünzli, *J. Alloys Compd.* **2006**, *408–412*, 934.

[9] T. Lazarides, H. Adams, D. Sykes, S. Faulkner, G. Calogero, M. Ward, *Dalton Trans.* **2008**, 691; D. Imbert, M. Cantuel, J.-C. G. Bünzli, G. Bernardinelli, C. Piguet, *J. Am. Chem. Soc.* **2003**, *125*, 15698; J. W. Stouwdam, M. Raudsepp, F. C. J. M. van Veggel, *Langmuir* **2005**, *21*, 7003.

[10] N. K. Al-Rasbi, C. Sabatini, F. Barigelletti, M. D. Ward, *Dalton Trans.* **2006**, 4769; C. G. Gulgas, T. M. Reinecke, *Inorg. Chem.* **2008**, *47*, 1548.

[11] L. N. Puntus, K. A. Lyssenko, M. Y. Antipin, J.-C. G. Bünzli, *Inorg. Chem.* **2008**, *47*, 11095.

[12] L. N. Puntus, K. A. Lyssenko, I. S. Pekareva, J.-C. G. Bünzli, *J. Phys. Chem. B* **2009**, *113*, 9265.

[13] L. Puntus, K. Lyssenko, *J. Rare Earths* **2008**, *26*, 146.

[14] A. F. Kirby, D. Foster, F. S. Richardson, *Chem. Phys. Lett.* **1983**, *95*, 507; A. F. Kirby, F. S. Richardson, *J. Phys. Chem.* **1983**, *87*, 2544.

[15] T. Ikeyama, N. Okabe, T. Azumi, *J. Phys. Chem. A* **2001**, *105*, 7144.

[16] N. Sabbatini, M. Guardigli, J.-M. Lehn, *Coord. Chem. Rev.* **1993**, *123*, 201.

[17] M. Kleinerman, *J. Chem. Phys.* **1969**, *51*, 2370.

[18] S. I. Klink, L. Grave, D. N. Reinhoudt, F. C. J. M. van Veggel, M. H. V. Werts, F. A. J. Geurts, J. W. Hofstraat, *J. Phys. Chem. A* **2000**, *104*, 5457.

[19] A. J. Bard, R. Parsons, J. Jordan, 'Standard Potentials in Aqueous Solution', Marcel Dekker Inc., New York, 1985.

[20] R. Demirbilek, J. Heber, S. I. Nikitin, *Proc. SPIE* **2002**, *4766*, 47.

[21] C. K. Jørgensen, *Mol. Phys.* **1962**, *5*, 271.

[22] M. H. V. Werts, R. T. F. Jukes, J. W. Verhoeven, *Phys. Chem. Chem. Phys.* **2002**, *4*, 1542.

[23] M. Latva, H. Takalo, V.-M. Mukkala, C. Matachescu, J. C. Rodríguez-Ubis, J. Kankare, *J. Lumin.* **1997**, *75*, 149.

[24] N. Sabbatini, S. Perathoner, G. Lattanzi, S. Dellonte, V. Balzani, *J. Phys. Chem.* **1987**, *91*, 6136; F. J. Steemers, H. G. Meuris, W. Verboom, D. N. Reinhoudt, *J. Org. Chem.* **1997**, *62*, 4229.

[25] J. R. Lakowicz, 'Principles of Fluorescence Spectroscopy', 2nd ed., Kluwer Academic, New York, 1999, pp. 95–140.

Received May 4, 2009